Available online at www.sciencedirect.com
ScienceDirect
Journal of Organometallic Chemistry 691 (2006) 4633–4640
Journal of Organometallic Chemistry
www.elsevier.com/locate/jorganchem

# Tris(*N*-pyrrolidinyl)phosphine substituted diiron dithiolate related to iron-only hydrogenase active site: Synthesis, characterization and electrochemical properties

Jun Hou [a], Xiaojun Peng [a,*], Zhiyou Zhou [b], Shigang Sun [b], Xing Zhao [a], Shang Gao [a]

[a] *State Key Laboratory of Fine Chemicals, Dalian University of Technology, 116012 Dalian, PR China*
[b] *State Key Laboratory for Physical Chemistry of Solid Surface, Xiamen University, 361005 Xiamen, PR China*

Received 15 May 2006; received in revised form 3 July 2006; accepted 11 July 2006
Available online 18 July 2006

**Abstract**

A tris(*N*-pyrrolidinyl)phosphine ($P(NC_4H_8)_3$) monosubstituted complex, $[(\mu\text{-pdt})Fe_2(CO)_5P(NC_4H_8)_3]$ (**2**) was synthesized as a functional model of the hydrogen-producing capability of the iron hydrogenase active site. The structure was fully characterized by X-ray crystallography. IR and electrochemical studies have indicated that the $P(NC_4H_8)_3$ ligand has better electron-donating ability than that of those phosphine ligands, such as $PMe_3$, PTA (1,3,5-triaza-7-phosphaadamantane), $PMe_2Ph$ $PPh_3$, and $P(OEt)_3$. The electrocatalytic activity of **2** was recorded in $CH_3CN$ in the absence and presence of weak acid, HOAc. The cathodic shift of potential at −1.98 V and the dependence of current on acid concentration have indicated that complex **2** can catalyze the reduction of protons to hydrogen at its $Fe^0Fe^I$ level in the presence of HOAc. IR spectroelectrochemical experiments are conducted during the reduction of **2** under nitrogen and carbon monoxide, respectively. The formation of a bridging CO group during the reduction of **2** at −1.98 V has been identified using IR spectroelectrochemical techniques, and an electrocatalytic mechanism of **2** consistent with the spectroscopic and electrochemical results is proposed.


*Keywords:* Bioinorganic chemistry; Fe-only hydrogenase; Spectroelectrochemistry; Phosphine ligand

## 1. Introduction

Homogeneous catalysts for proton reduction to hydrogen [1], especially those derived from more economically base metals iron, have drawn considerable attention of chemists in the past years because of their potential for replacing expensive platinum-containing catalysts [2]. The iron-only hydrogenases, $[Fe]H_2$ases, can catalyze the formation of hydrogen at extraordinarily high rates utilizing base metal iron, [3–5] according to the reaction $2H^+ + 2e^- \rightleftarrows H_2$. The active site of $[Fe]H_2$ases, wherein the catalytic chemistry takes place, is composed of a diiron unit linked to a cysteine-S bridged $[Fe_4S_4]$ cluster which is determined by X-ray crystallographic [6,7] and spectroscopic [8,9] studies. The diiron subunit adopts a bi-octahedral butterfly geometry, which each Fe atom is coordinated by unusual ligands, CO and $CN^-$ (Fig. 1a).

Because of high efficiency of $[Fe]H_2$ases, as well as the simple structure of the active site resembling well-known organometallic complexes $Fe_2(\mu\text{-SR})_2(CO)_{6-\chi}L_\chi$, a number of structural [10–13] and functional [14–16] model complexes for the active site of $[Fe]H_2$ases have been prepared in the past years. In this context, the good electron-donating phosphine substituted diiron derivatives are particular interest in the development of catalysts for $H_2$ electrolysis (Fig. 1b) [14b,14c,15a,15b] for these phosphine ligands enhance the electron density and therefore render diiron center more nucleophilic. Recently, Darensbourg and

* Corresponding author. Tel.: +86 411 88993899; fax: +86 411 88993906.
*E-mail address:* Pengxj@dlut.edu.cn (X. Peng).

0022-328X/$ - see front matter © 2006 Elsevier B.V. All rights reserved.
doi:10.1016/j.jorganchem.2006.07.010

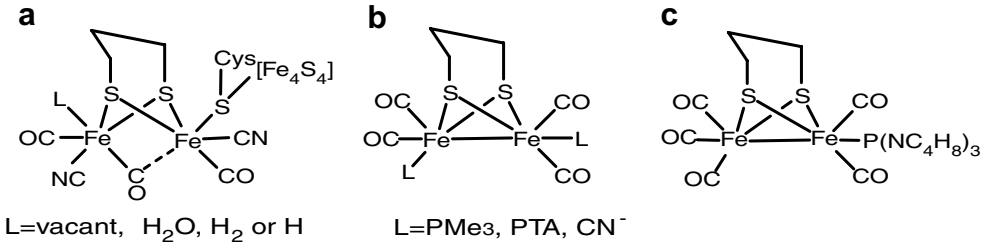


Fig. 1. The active site of [Fe]$H_2$ases (a), electrocatalysts for $H_2$-production (b), and an asymmetrically substituted model complex (c).

co-workers have described that the asymmetrically monosustituted diiron complex [(μ-pdt)$Fe_2(CO)_5$PTA], **1-PTA**, is the most effective electrocatalyst for proton reduction in the presence of weak acid, HOAc [14c]. Density functional theory (DFT) calculations suggest that an asymmetrically substituted diiron complex having a good electron-donating ligand favors the formation of a bridging CO group through the transformation of a CO ligand from terminal to bridging binding [17–19]. We have been wondering if the active transition of the asymmetric diiron model complexes during electrocatalysis has such CO-bridged conformation. We have thus prepared tris(*N*-pyrrolidinyl)phosphine monosubstituted diiron compound **2**, [(μ-pdt)$Fe_2(CO)_5P(NC_4H_8)_3$] (Fig. 1c), and described the investigation of the electrochemical and spectroelectrochemical properties of complex **2**. The formation of a bridging CO group during one-electron reduction of **2** has been identified using IR spectroelectrochemical techniques. The electrochemical response of **2** in the absence and presence of weak acetic acid, HOAc, is examined by cyclic voltammograms, and it is shown that this model system is electrocatalytically active in terms of proton reduction.

## 2. Results and discussion

### 2.1. Preparation and spectroscopic characterization of 2

The complex **2** was readily prepared in a good yield by reaction of **1** and $P(NC_4H_8)_3$ in refluxing toluene, which afforded a dark red solution. The product was isolated by column chromatography on $Al_2O_3$. The details of synthesis and isolation are described in experimental section. Three major CO bands at 2034, 1973, 1912 $cm^{-1}$ were observed in IR spectrum. $^{31}P$ NMR showed a single signal at 132.57 ppm. The product obtained was further characterized by $^1H$ & $^{13}C$ NMR spectroscopy, and HR-MS. The HR-MS analysis is in good agreement with the supposed molecular weight. The complex is stable to air and thermally stable.

### 2.2. Molecular structure of 2 in solid state

The overall structure of **2** is shown in Fig. 2 and selected bond lengths and angles are listed in Table 1. The geometry of **2** is nearly identical with that of those tertiary phosphine-monosubstituted derivatives [(μ-pdt)$Fe_2(CO)_5$L], (L = $PMe_3$, $PMe_2Ph$, $PPh_3$, $P(OEt)_3$ [20]. Different from those tertiary phosphine ligands in apical positions [20], the $P(NC_4H_8)_3$ ligand of **2** is in basal position and roughly *cis* to the Fe–Fe bond, similar to that of **1-PTA** [14c]. This arrangement may minimize the $P(NC_4H_8)_3$ ligand steric interactions with the six-membered ring of propanedithiolate. The Fe–Fe distance of 2.5527(9) Å in **2** is enlarged by ca. 0.01–0.04 Å than those found in phosphine momosubstituted complexes [(μ-pdt)$Fe_2(CO)_5$L] [20], and nearly identical with those in disubstituted complexes [(μ-pdt)$Fe_2(CO)_4(PMe_3)_2$] [21] and [(μ-pdt)$Fe_2(CO)_4PTA_2$] [14c]. This suggests that $P(NC_4H_8)_3$ ligand has better

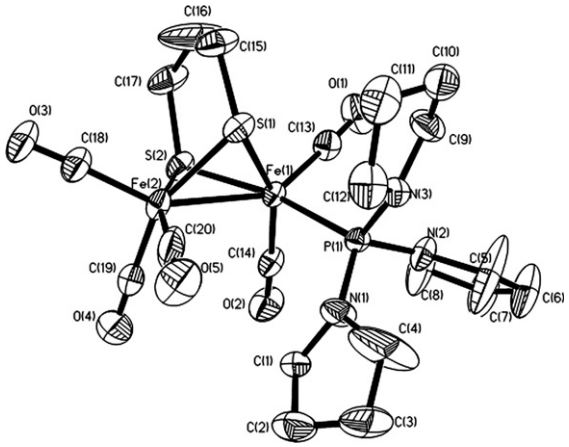


Fig. 2. ORTEP (ellipsoids at 30% probability level) view of **2**.

Table 1
Selected bond lengths [Å] and angles [°] for **2**

| | | | |
|---|---|---|---|
| Fe(1)–Fe(2) | 2.5527(9) | Fe(1)–S(1)–Fe(2) | 69.19(4) |
| Fe(1)–S(1) | 2.2418(12) | Fe(1)–S(2)-Fe(2) | 68.61(4) |
| Fe(1)–S(2) | 2.2675(11) | S(1)–Fe(1)–S(2) | 84.56(4) |
| Fe(2)–S(1) | 2.2542(14) | S(1)–Fe(2)–S(2) | 84.41(5) |
| Fe(2)–S(2) | 2.2615(14) | C(15)–S(1)–Fe(1) | 112.5(2) |
| Fe(1)–P(1) | 2.2563(11) | C(17)–S(2)–Fe(2) | 110.4(2) |
| Fe(1)–C(13) | 1.765(5) | P(1)–Fe(1)–Fe(2) | 111.61(4) |
| P(1)–N(1) | 1.662(4) | C(20)–Fe(2)–Fe(1) | 105.0(3) |
| P(1)–N(2) | 1.670(4) | C(13)–Fe(1)–Fe(2) | 146.67(16) |
| P(1)–N(3) | 1.682(3) | C(18)–Fe(2)–Fe(1) | 148.2(2) |
| | | N(1)–P(1)–N(2) | 109.1(2) |
| | | N(1)–P(1)–N(3) | 100.4(2) |
| | | N(2)–P(1)–N(3) | 100.4(2) |

electron-donating ability. The bond length of Fe–Fe in **2** is very close to the corresponding lengths (2.60 Å) of the iron hydrogenase enzymes [6,7]. The Fe–P distance of 2.2563(11) Å is in good agreement with those in phosphine-coordinating diiron compounds [14c,20,21].

The geometries of nitrogen heteroatoms in $P(NC_4H_8)_3$ ligand are notable. The $P(NC_4H_8)_3$ ligand shares two nearly planar nitrogen atoms (N1 and N2) and a pyramidal nitrogen (N3). The sum of C–N–C angles around N1 and N2 are 355° and 357°, respectively, while the sum of C–N–C angle around N3 is 351°. The configuration at nitrogen atoms resembles the situation in other $P(NC_4H_8)_3$-substituted metal carbonyl complexes [20]. The N–P bond length of 1.682(3) Å involving the pyramidal nitrogen is slightly longer than those in the planar nitrogens which the corresponding values of *N*–P bond are 1.662(4) Å for N1–P1, 1.670(4) Å for N2–P1, respectively. This bond length feature is also observed for those $P(NC_4H_8)_3$-substituted complexes [22].

### 2.3. Donor ability of $P(NC_4H_8)_3$ ligand

The IR spectra of CO bands are considered as a useful tool for evaluating the electron-donating abilities of ligands of metal carbonyl complexes. For comparison purposes, IR data of CO bands for **1**, and its phosphine-monosubstituted complexes **2** ($L = P(NC_4H_8)_3$), **3** ($L = PMe_3$), **4** (L = PTA), **5** ($L = PMe_2Ph$), **6** ($L = PPh_3$) and **7** ($L = P(OEt)_3$), were summarized in Table 2. As can be seen in Table 2, the IR spectrum of **2** in $CH_3CN$ shows three major bands in CO region at 2034, 1973, 1912 $cm^{-1}$ which shifts to lower frequencies by an average value ca. 55 $cm^{-1}$ as compared with the parent complex **1**. Whereas the three-band patterns in the $\nu_{(CO)}$ region for complexes **2** and **3** are almost identical, an average shift of 10 $cm^{-1}$ for the former to lower wavenumber indicates that $P(NC_4H_8)_3$ has better electron-donating ability vs $PMe_3$ ligand. The value of $\nu_{(CO)}$ for **2** is significantly lower than those of other highly electron rich phosphine (compares complexes **4**, **5**, **6** and **7**). Thus, the electron-donating capabilities of these phosphine ligands exhibit the following ranking: $P(NC_4H_8)_3 > PMe_3 > PTA > PMe_2Ph > PPh_3 > P(OEt)_3$. In view of the bond lengths of P–N in **2**, the better electron-donating ability of $P(NC_4H_8)_3$ ligand can be attributed to the donation towards phosphorus atom from lone pair electron of two planar nitrogens [22,23]. The proposed electronic donation of $P(NC_4H_8)_3$ ligand is shown in Fig. 3.

Table 2
A comparison of CO bands of $[(\mu\text{-pdt})Fe_2(CO)_5L]$

| Complex | L | $\nu_{(CO)}$ [$cm^{-1}$] | Note |
|---|---|---|---|
| **1** | CO | 2074 (m), 2036 (s), 1995 (s) | Ref. [14b] |
| **2** | $P(NC_4H_8)_3$ | 2034 (s), 1973 (s), 1912 (m) | This work |
| **3** | $PMe_3$ | 2037 (s), 1980 (s), 1919 (m) | Ref. [20] |
| **4** | PTA | 2038 (s), 1983 (*vs*), 1928 (m) | Ref. [14c] |
| **5** | $PMe_2Ph$ | 2040 (s), 1980 (s), 1921 (m) | Ref. [20] |
| **6** | $PPh_3$ | 2044 (s), 1984 (s), 1931 (m) | Ref. [20] |
| **7** | $P(OEt)_3$ | 2046 (s), 1989 (s), 1936 (m) | Ref. [20] |

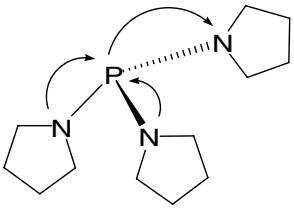


Fig. 3. The proposed donor properties of $P(NC_4H_8)_3$ ligand.

### 2.4. Electrochemistry of **2**

The phosphine-monosubstituted diiron complexes, $[(\mu\text{-pdt})Fe_2(CO)_5L]$, ($L = PMe_3$, PTA, $PMe_2Ph$, $PPh_3$, $P(OEt)_3$) have been reported to undergo an electrochemically irreversible reduction at moderately negative potentials depending on the electron-donating abilities of ligands in diiron core [20,14b,14c]. The cyclic voltammogram of **2** shown in Fig. 4a was recorded in $CH_3CN$ solution (with 0.1 M *n*-$Bu_4NPF_6$ as electrolyte), it was initiated from the open circuit and proceeds in a cathodic direction. Complex **2** displays an electrochemically irreversible reduction at −1.98 V vs $Fc^+/Fc$. Bulky electrolysis of **2** at −1.98 V demonstrates a net consumption ~0.93 electron per molecule. This suggests that the reduction event at −1.98 V is a one-electron reduction process, assigned to

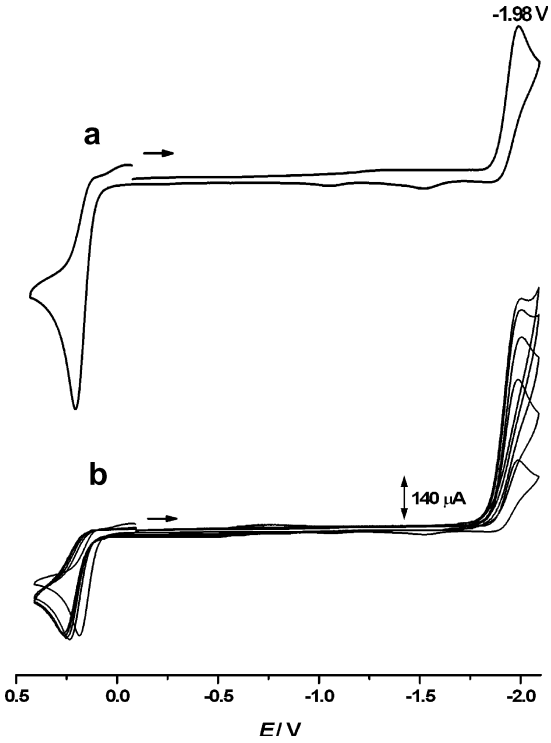


Fig. 4. Cyclic voltammograms of **2** (1 mM) in $CH_3CN$ (0.1 M *n*-$Bu_4NPF_6$) at a potential scan rate of 100 mV $s^{-1}$, (a) in the absence of HOAc; (b) in the presence of HOAc (0, 5, 10, 20 and 30 mM).

the $Fe^{I}Fe^{I} + e^{-} \rightarrow Fe^{I}Fe^{0}$ couple, as previously reported for the all-CO parent complex **1** and its phosphine-coordinated diiron derivatives [20,14b,14c]. The second reduction event of **2** is not observed within the electrochemical window of solvent in Fig. 4. The anodic peak observed at $E_p^{ox} = 0.18$ V is attributed to the oxidative couple $Fe^{I}Fe^{I}/Fe^{I}Fe^{II}$. Compared with the parent complex **1**, the $Fe^{I}Fe^{I}/Fe^{I}Fe^{0}$ couple and $Fe^{I}Fe^{I}/Fe^{I}Fe^{II}$ couple of **2** are shifted in a cathodic direction, consistent with the increase of electron density in diiron center as a CO is replaced by a better σ-donor phosphine ligand. It is instructive to compare the cyclic voltammograms of **2** with PTA-substituted analogue, **1-PTA**. For the latter, the first reduction event assigned to the $Fe^{I}Fe^{I}/Fe^{I}Fe^{0}$ couple is at $E_p^{red} = -1.54$ V versus NHE (corresponding to −1.94 V versus $Fc^{+}/Fc$) [14c]. The potential shift of **2** by 40 mV to a more negative value further indicates the better donor feature of $P(NC_4H_8)_3$ relative to PTA ligand. The peak current of these redox couples is proportional to the square root of the scan rate (50–500 mV $s^{-1}$), which suggests that the electrochemical processes are diffusion-controlled [24].

### 2.5. Electrocatalytic proton reduction in $CH_3CN$ solution

Although a number of phosphine-monosubstituted propanedithiolate diiron complexes have been prepared, it is of particular interest that only one compound, **1-PTA**, was utilized to study the electrocatalytic proton reduction to date [14c]. Here we describe the proton electroreduction catalyzed by **2** in the presence of weak proton acid, HOAc (5–30 mM), using cyclic voltammogram (Fig. 4b). when 5 mM of HOAc was added, a drastic increase in the current intensity of the reduction wave at −1.98 V was observed, and the corresponding reduction potential shifted by 10 mV in a cathodic direction. The height of the reduction peak at −1.98 V showed a further significant increase with the sequential increments of acid concentration, and the potential shifts to a more negative value. That is, the first reduction event at −1.98 V is significantly sensitive to the acid concentration. The current height of the cathodic peak at −1.98 V for **2**, derived from results in Fig. 4b, displays a good linear dependence on the concentration of HOAc. These features are indicative of catalytic proton reduction [25]. Thus, the first reduction event at −1.98 V is electrocatalytically active in terms of proton reduction. Similar features were observed in the electrocatalytic proton reduction by **1-PTA** in the presence of HOAc [14c].

Further evidence for the electrocatalytic proton reduction to $H_2$ was obtained by bulk electrolysis of a $CH_3CN$ solution of **2** (2.5 mM) with HOAc (100 mM) at −2.10 V, a potential slightly beyond the first reduction peak. After 1 h, the total charge passed through the cell approaches 12 F per mol of **2**, which is equivalent to 6 turnover. In such a preparative scale experiment, dihydrogen was obtained. Analysis of gas chromatography showed dihydrogen was a sole gaseous product.

### 2.6. IR Spectroelectrochemistry (SEC) investigation of the reduction of 2

The $\nu_{(CO)}$ bands in IR spectra provide a useful method for assessing the electronic and structural changes at metal centers by IR spectroelectrochemistry [26]. To further uncover the catalytic mechanism of **2**, reduction of **2** at a applied potential at −1.98 V was investigated by IR spectroelectrochemical technique in CO and $N_2$-saturated THF solution. The IR spectral changes in CO region during the electrochemical reduction of **2** in a thin-layer IR cell were shown in Fig. 5. For comparison purposes, the IR spectrum of **2** prior to the application of the potential is included (Fig. 5a). Upon reduction of 10 mM **2** in THF

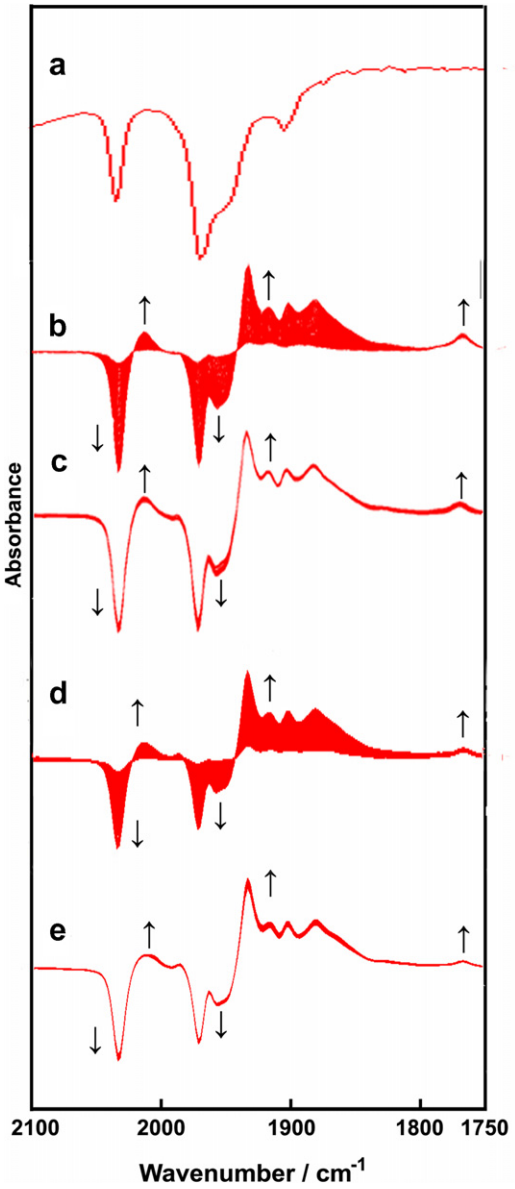


Fig. 5. IR spectra in the CO region recorded during the reduction of 10 mM **2** in THF (0.1 M *n*-$Bu_4NPF_6$) in the SEC cell at −1.98 V. (a) In CO-saturated solution prior to the application of the potential; (b, c) in CO-saturated solution; (d, e) in $N_2$-saturated solution.

solution under carbon monoxide, the three major $\nu_{(CO)}$ IR bands at 2034, 1974 and 1953 $cm^{-1}$ of the starting material display a loss of intensity, with the growth of bands at lower frequencies with 2014, 1938, 1921, 1908 and 1888 $cm^{-1}$ (Fig. 5b and c). These bands at lower wavenumbers can be attributed to the terminal CO ligands coordinated to two Fe atoms of the diiron unit, which their frequencies are in good agreement with terminal CO stretching modes of iron carbonyl complexes [26]. As compared with the IR bands of terminal CO ligands of **2** (Fig. 5), an shift of the $\nu_{(CO)}$ bands of one-electron reduced species **2B** on average ca. 30 $cm^{-1}$ to lower energy is consistent with electron density being added to the $\pi^*_{(CO)}$ orbitals. Whereas the carbonyl stretching frequencies shift to lower wavenumbers, the major $\nu_{(CO)}$ bands of **2B** are similar to those of **2**. Interestingly, the IR bands of terminal CO ligands of **2B** show a significant similarity to those of the one-electron reduced species $[(\mu\text{-pdt})Fe_2(CO)_6]^-$ [27], generated by the reduction of complex $[(\mu\text{-pdt})Fe_2(CO)_6]$.

It was noteworthy that a peak at 1778 $cm^{-1}$ was observed during the reduction of **2** (Fig. 5b and c). On the basis of its low frequency at 1778 $cm^{-1}$, this band can be assigned as a bridging CO ligand [26], which typically bonds to both iron atoms via coordination through the carbon of CO group and shows significantly lower frequencies than those of terminally coordinated CO ligands. In support of this assignment, we note that the synthetic diiron model complexes reported by Rauchfuss et al., [28–30] and phosphido-bridged diiron complex, $[(\mu\text{-}PPh_2)_2HFe_2(\mu\text{-CO})(CO)_5]^-$ [31], displayed similar bridging CO frequencies. Of particular significance is the fact that this band detected is closely related to that reported cyano-substituted {**2Fe3S**} derivative having a bridging CO group of $\nu_{(CO)} = 1780$ $cm^{-1}$ due to the a thioether coordinated to one iron [11a].

The well-defined spectral changes suggest that the electrochemical reduction of CO-saturated solution of **2** results in a near quantitative species by a one-electron reduction with no obvious buildup of additional products. The final spectrum obtained following the reduction of **2** is nearly attributed to **2B** with no contribution of **2** (Fig. 5c), indicating **2** completely converts into **2B**. Reoxidation of the reduced film of solution containing **2B** even at −300 mV only gave a small quantity of **2** (not shown), consistent with the electrochemically irreversible reduction of **2** at −1.98 V.

For a comparison purpose, IR spectra changes in SEC experiments upon reduction of **2** in $N_2$-saturated solution (Fig. 5d and e) were also recorded under same conditions. Although the IR spectra obtained in $N_2$-saturated solution are similar to those recorded in CO-saturated solution (Fig. 5b and c), the conversion rate of **2** to **2B** in $N_2$-saturated solution is faster than that recorded in CO-saturated solution. A typical plot of conversion rate of **2** to **2B** as given at 2014 $cm^{-1}$ under CO and $N_2$ atmosphere was shown in Fig. 6. Maybe either additional CO impedes the formation of one-electron reduced species or CO reacts

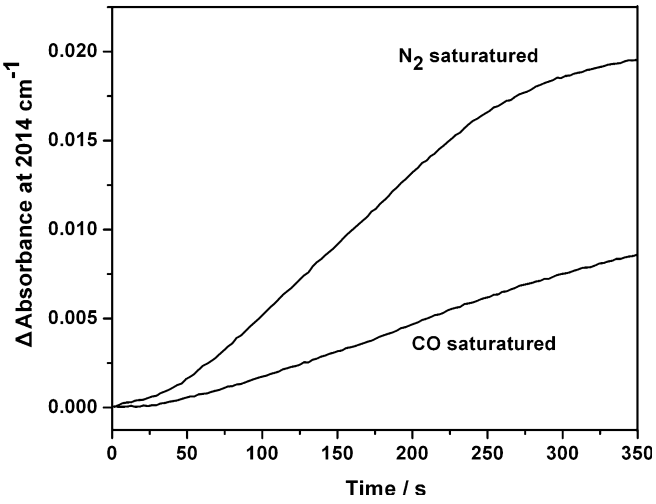


Fig. 6. Rate of conversion of **2** into **2B** from CO and $N_2$-saturated solution (as given by Δ absorbance at 2014 $cm^{-1}$).

with the transient intermediate to inhibit the efficient conversion into **2B**.

In view of the similarity in IR spectra of the terminal and bridging CO ligands, the structure of **2B** with a bridging CO group can be suggested. A reasonable interpretation for the formation of a bridging CO group is that an asymmetrical charge distribution and the structural asymmetry at the two iron centers due to the coordination of an electron-donating $P(NC_4H_8)_3$ ligand make the rotation of $Fe(CO)_3$ unit when diiron center is reduced. A more electron-rich $Fe(CO)_2P(NC_4H_8)_3$ unit favors the transformation of CO ligand in $Fe(CO)_3$ unit from terminal to bridging binding. Excessive electron density could be transferred to $Fe(CO)_3$ unit through a bridging CO bond, which stabilizes of one-electron reduced species $Fe^0Fe^I$. In addition, the strong electron-donating ability of $P(NC_4H_8)_3$ ligand facilitates the stability of the conformation of a CO bridging group. These concerted electronic and structural changes, which are aimed at the formation of a CO-bridged geometry, have been proposed for the asymmetric diiron complexes by DFT calculations [17–19]. In fact, Pickett et al. have presented IR spectroscopic data for μ-CO group in {**2Fe3S**} in which one of the CO ligands is rotated into a bridging binding with $CN^-$ substitution of CO [11a,11b]. Our results confirm the formation of a bridging CO group during electrocatalytic $H_2$-production by an asymmetrically substituted diiron complex having a good electron-donating ligand.

For these results described above for cyclic voltammograms and SEC experiments, an ECCE mechanism for the electrocatalytic proton reduction of **2** could be proposed, as described in Scheme 1. Complex **2** initially undergoes an electrochemical reduction to generate a one-electron reduced intermediate **2A**. The transition **2A** rapidly converts into a CO-bridged species **2B**. After double protonation of **2B** and a second electroreduction event, hydrogen is evolved, and the starting material is reclaimed

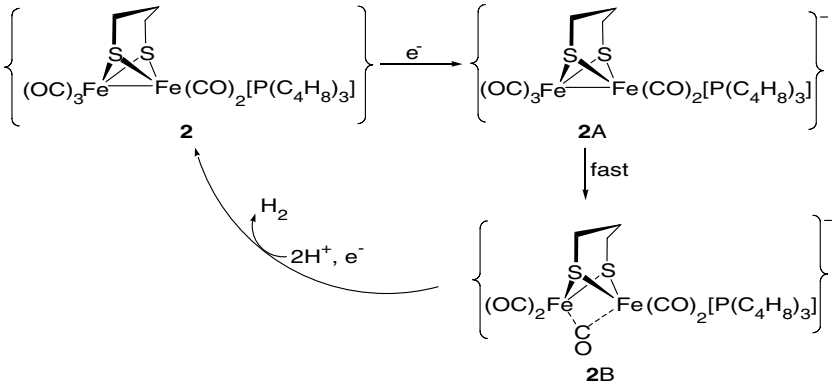


Scheme 1. A possible electrocatalytic mechanism for **2**.

to fulfill the catalytic cycle. A similar mechanism was proposed for $H_2$ production by PTA-substituted diiron complex, **1-PTA** [14c]. Our results also show that a reductive $Fe^0Fe^I$ of **2** is electrocatalytically active. This further suggests that the asymmetrically monosubstituted diiron derivatives have more potential in the development of electrocatalysts for $H_2$-evolution.

Although there is no spectroscopic evidence for the detailed geometry of **2B** and for proton-binding intermediate, we show that the formation of a bridging CO group is a crucial process during electrocatalytic proton reduction.

## 3. Conclusion

An asymmetric tris(*N*-pyrrolidinyl)phosphine monosubstituted diiron complex **2** was prepared as a biomimetic organometallic model related to the active site of iron-only hydrogenase. The IR spectroscopy and cyclic voltammogram of **2** indicate that the introduction of the $P(NC_4H_8)_3$ ligand does enhance the electron density in diiron core. As compared with the IR spectra of complexes **3**–**7**, the $P(NC_4H_8)_3$ ligand in **2** has significant electronic influence of the CO frequencies. In comparison with phosphine monosubstituted diiron complex **1-PTA**, complex **2** shifts the first reduction peak to a more negative value. The better donor ability of $P(NC_4H_8)_3$ ligand is contributed from the lone pair electron of the nitrogen heteroatoms in two pyrrolidines.

In the presence of weak acid, HOAc, complex **2** can catalyze the reduction of protons to $H_2$. The first reduction level $Fe^0Fe^I$ is electrochemically active, which is similarly rapid as complex **1-PTA**. An ECCE mechanism is tentatively proposed for the electrocatalytic proton reduction in the presence of HOAc.

A noteworthy result is that the formation of a bridging CO group is identified by IR SEC during the reduction of **2**, which is assumed to play a key role in electrocatalytic $H_2$-production. An asymmetry at two diiron centers maybe favors the transformation of CO ligand from terminal to bridging binding. This work also shows the formation of a CO bridge is a reasonable activation step in the enzymatic $H_2$-evolution process. In terms of the mechanism of electrocatalytic proton reduction by **2**, studies on the mode of hydride binding and the influence of better donor ligands on coordination geometry are needed in future work, which will enable us to further understand the electrocatalytic mechanism of such asymmetrically substituted diiron models.

## 4. Experimental

### 4.1. Materials and techniques

All reactions and operations were carried out under $N_2$ atmosphere using standard Schlenk techniques. All solvents were dried and distilled prior to use according to the standard methods. The following materials were commercially chemicals and used without further purification: 1,3-propanedithiol, pyrrolidine, $PCl_3$, $[Fe(CO)_5]$. The starting materials tris(*N*-pyrrolidinyl)phosphine and $(\mu\text{-pdt})Fe_2(CO)_6$ were synthesized according to the literature procedures [22,32].

Infrared spectra were recorded on a FT-IR spectrophotometer. $^1H$, $^{13}C$ and $^{31}P$ NMR were collected on a Varian INOVA 400 NMR spectrometer, $^{31}P$ NMR spectra were referenced relative to $H_3PO_4$. HR-MS spectra determinations were made on a GCT-MS instrument (Micromass, England).

### 4.2. Synthesis of $[(\mu\text{-pdt})Fe(CO)_5P(NC_4H_8)_3]$, 2

To a red solution of $(\mu\text{-pdt})Fe_2(CO)_6$, **1** (2 g, 5.18 mmol) in toluene (100 mL) was added via syringe the tris(pyrrolidinyl)phosphine (2.5 g, 10.4 mmol) in toluene (30 mL). The reaction mixture was refluxed until TLC indicated there was no remaining carbonyl complex of starting material. The solvent was removed under vacuum and the resulted dark red residue was purified by column chromatography on $Al_2O_3$ eluting with $CH_2Cl_2$/hexane (1:50, v/v). A red dark solid was obtained from recrystallization in $CH_2Cl_2$/hexane in 80% yield. Crystals suitable for X-ray studies were grown from a mixed $CH_2Cl_2$/hexane solution. IR

(in $CH_2Cl_2$): $\nu_{(CO)} = 2032$, 1969, 1910. $^1H$ NMR (ppm, $CDCl_3$): $\delta = 3.22$ (m, 12H), 2.25 (m, 2H), 1.93 (m, 4H), 1.85 (m, 12H). $^{13}C$ NMR (ppm, $CDCl_3$): $\delta = 216.5$, 216.3, 210.8, 48.4, 30.1, 26.4, 24.6. $^{31}P$ NMR ($CDCl_3$): $\delta = 132.57$ ppm. HR-MS (EI): (*m*/*z*) calc. for $[M]^+$: 599.0063; found: 599.0109.

### 4.3. X-ray structure determinations

The single-crystal X-ray data were collected on a Siemens SMART CCD diffractometer. The data were collected at 293 K using graphite monochromated Mo $K_\alpha$ radiation ($\lambda = 0.71073$ Å) under $\omega - 2\theta$ scan mode. Data processing was accomplished with the SAINT processing program [33]. Intensity data were corrected for absorption with empirical methods. The structure was solved by direct methods and refined on $F_o^2$ against full-matrix least-squares by the SHELXTL 97 program package [34]. All of the non-hydrogen atoms were refined anisotropically. Hydrogen atoms were located by geometrical calculation, but their positions and thermal parameters were fixed during the structure refinement. A summary of the crystallographic data and structural determinations is provided in Table 3. CCDC-603054 (**2**) contains the supplementary crystallographic data for this paper. These data can be obtained free of charge via www.ccdc.cam.ac.uk/conts/retrieving.html (or from the Cambridge Crystallographic Data Centre, 12 Union Road, Cambridge CB21EZ, UK; fax: (+44) 1223-336-033; or e-mail: deposit@ccdc. cam.ac.uk).

Table 3
X-ray crystallographic data for **2**

| | **2** |
|---|---|
| Formula | $C_{20}H_{30}Fe_2N_3O_5PS_2$ |
| Mr [g mol$^{-1}$] | 599.26 |
| $\lambda$ [Å] | 0.71073 |
| Crystal system | Monoclinic |
| Space group | *P*21/c |
| *a* [Å] | 17.870(4) |
| *b* [Å] | 9.154(2) |
| *c* [Å] | 16.904(4) |
| $\alpha$ [°] | 90.00 |
| $\beta$ [°] | 110.231(3) |
| $\gamma$ [°] | 90.00 |
| *V* [Å$^3$] | 2594.5(10) |
| *Z* | 4 |
| *T* [K] | 293 |
| $\rho_{calcd}$ [g cm$^{-3}$] | 1.534 |
| $\mu$ [mm$^{-1}$] | 1.376 |
| *F* [000] | 1240 |
| Total reflections | 6177 |
| Reflections observed | 4747 |
| Parameters | 298 |
| Goodness-of-fit on $F^2$ | 1.049 |
| $R_1$ [$I > 2\sigma(I)$] | 0.0641[a] |
| $\omega R_2$ [$I > 2\sigma(I)$] | 0.1808[b] |
| Maximum peak/hole [e Å$^{-3}$] | 2.569/−1.095 |

[a] $R_1 = (\sum ||F_o| - |F_c||)/(\sum |F_o|)$.
[b] $wR_2 = [\sum w(F_o^2 - F_c^2)^2 / \sum w(F_o^2)^2]^{1/2}$.

### 4.4. Electrochemistry

Acetonitrile used for electrochemical measurements was distilled once from $CaH_2$ and once from $P_2O_5$ and freshly distilled from $CaH_2$ under $N_2$. Measurements were made using a BAS 100W electrochemical workstation. All cyclic voltammograms were obtained in a conventional three-electrode cell under argon and room temperature. The working electrode was a glassy carbon disk (diameter 3 mm) successively polished with 3- and 1-μm alumina and sonicated in ion-free water for 15 min prior to use. The supporting electrolyte was 0.1 M *n*-$Bu_4NPF_6$ (Fluka, electrochemical grade). The experimental reference electrode was a non-aqueous $Ag/Ag^+$ electrode (0.01 M $AgNO_3$/0.1 M *n*-$Bu_4NPF_6$ in $CH_3CN$). All potentials are reported relative to the $Fc^+/Fc$. The counter electrode was platinum wire. During the electrocatalytic experiments under argon, increments of acid were added by microsyringe. Bulk electrolysis experiment was performed under argon atmosphere with a BAS 100W electrochemical analyzer, which was carried out on a glassy carbon rod ($A = 3.14$ cm$^2$) in a gastight H-type electrolysis cell containing ca. 16 mL of $CH_3CN$ solution. Gas chromatography was performed using a GC 920 instrument equipped with a thermal conductivity detector (TCD) under isothermal conditions with argon as a carrier gas.

### 4.5. Spectroelectrochemistry (SEC)

*In situ* FTIR experiments were carried out with a Nexus 870 FTIR spectrometer (Nicolet) equipped with a liquid-nitrogen cooled MCT-A detector. A model 263 A potentiostat/galvanostat (EG&G) was used to control electrode potential. The SEC experiments were performed by using a purpose-designed reflection-absorption cell in $N_2$ or CO-saturated THF solution as described previously [35]. The working electrode was a glassy carbon of 5 mm in diameter, the counter electrode was a platinum foil. The reference electrode ($Ag/Ag^+$) was separated from the bulk of the solution by a fritted-glass bridge of low porosity, which contained the solvent/supporting electrolyte mixture.

The IR-SEC spectra were collected in single beam mode at 2 cm$^{-1}$, and differential absorbance spectra were presented against the reference spectrum recorded immediately prior to the application of the potential.

## Acknowledgements

We are grateful to the Ministry of Education of China and National Natural Science Foundation of China (Projects 20128005, 20376010, and 20472012). Helpful discussions with Professor Zhongqun Tian are gratefully acknowledged. We also thank Dr. Yunling Gao, a former member of our group, solved the crystal structure of **2**.

## Appendix A. Supplementary data

Supplementary data associated with this article can be found, in the online version, at doi:10.1016/j.jorganchem.2006.07.010.

## References


[1] U. Koelle, New. J. Chem. 16 (1992) 157.
[2] R. Cammack, Nature 397 (1999) 214.
[3] M.W.W. Adam, Biochim. Biophys. Acta 1020 (1990) 115.
[4] J.W. Peters, Curr. Opin. Struct. Biol. (1999) 670.
[5] M. Frey, ChemBioChem. 3 (2002) 152.
[6] J.W. Peters, W.N. Lanzilotta, B.J. Lemon, L.C. Seefeldt, Science 282 (1998) 1853.
[7] Y. Nicolet, C. Piras, P. Legrand, C.E. Hatchikian, J.C. Fontecilla-Camps, Structure 7 (1999) 13.
[8] A.L. De Lacey, C. Stadler, C. Cavazza, E.C. Hatchikian, V.M. Fernandez, J. Am. Chem. Soc. 122 (2000) 11232.
[9] Z. Chem, B.J. Lemon, S. Huang, D.J. Swartz, J.W. Peters, K.A. Bagley, Biochemistry 41 (2002) 2036.
[10] (a) M.Y. Darensbourg, E.J. Lyon, J.J. Smee, Coord. Chem. Rev. 206–207 (2000) 533;
(b) E.J. Lyon, I.P. Georgakaki, J.H. Reibenspies, M.Y. Darensbourg, Angew. Chem. In. Ed. 38 (1999) 3178;
(c) I.P. Georgakaki, M.L. Miller, M.Y. Darensbourg, Inorg. Chem. 42 (2003) 2489.
[11] (a) M. Razavet, S.C. Davies, D.L. Hughes, C.J. Pickett, Chem. Commun. (2001) 847;
(b) S.J. George, Z. Cui, M. Razavet, C.J. Pickett, Chem. Eur. J. 8 (2002) 4037;
(c) D.J. Evans, C.J. Pickett, Chem. Soc. Rev. 32 (2003) 268;
(d) C. Tard, X. Liu, S.K. Ibrahim, M. Bruschi, L.D. Gioia, S.C. Davies, X. Yang, L.-S. Wang, G. Sawers, C.J. Pickett, Nature 433 (2005) 610.
[12] (a) J.D. Lawrence, H. Li, T.B. Rauchfuss, Chem. Commun. (2001) 1482;
(b) J.D. Lawrence, H. Li, T.B. Rauchfuss, M. Bénard, M.-M. Rohmer, Angew. Chem. Int. Ed. 40 (2001) 1768;
(c) C.A. Boyke, T.B. Rauchfuss, S.R. Wilson, M.-M. Rohmer, M. Bénard, J. Am. Chem. Soc. 126 (2004) 15151;
(d) C.A. Boyke, J.I. van der Vlugt, T.B. Rauchfuss, S.R. Wilson, G. Zampella, L. De Gioia, J. Am. Chem. Soc. 127 (2005) 11010.
[13] (a) L. Song, Z. Yang, H. Bian, Q. Hu, Organometallics 23 (2004) 3082;
(b) F. Wang, M. Wang, X. Liu, K. Jin, W. Dong, G. Li, B. Åkermark, L. Sun, Chem. Commun. (2005) 3221.
[14] (a) X. Zhao, I.P. Georgakaki, M.L. Miller, J.C. Yarbrough, M.Y. Darensbourg, J. Am. Chem. Soc. 123 (2001) 9710;
(b) D. Chong, I.P. Georgakaki, R. Mejia-Rodriguez, J. Sanabria-Chinchilla, M.P. Soriaga, M.Y. Darensbourg, J. Chem. Soc. Dalton Trans. (2003) 4158;
(c) R. Mejia-Rodriguez, D. Chong, J.H. Reibenspies, M.P. Soriaga, M.Y. Darensbourg, J. Am. Chem. Soc. 126 (2004) 12004.
[15] (a) F. Gloaguen, J.D. Lawrence, T.B. Rauchfuss, J. Am. Chem. Soc. 123 (2001) 9476;
(b) F. Gloaguen, J.D. Lawrence, T.B. Rauchfuss, M. Bénard, M.-M. Rohmer, Inorg. Chem. 41 (2002) 6573.
[16] (a) S. Ott, M. Kritikos, B. Åkermark, L. Sun, R. Lomoth, Angew. Chem. Int. Ed. 43 (2004) 1006;
(b) T. Liu, M. Wang, Z. Shi, H. Cui, W. Dong, J. Chen, B. Åkermark, L. Sun, Chem. Eur. J. 10 (2004) 4474.
[17] M.Y. Darensbourg, E.J. Lyon, X. Zhao, I.P. Georgakaki, Proc. Natl. Acad. Sci. U.S.A. 100 (2003) 3683.
[18] M. Bruschi, P. Fantucci, L. De Gioia, Inorg. Chem. 43 (2004) 3733.
[19] J.W. Tye, M.Y. Darensbourg, M.B. Hall, Inorg. Chem. 45 (2006) 1552.
[20] P. Li, M. Wang, C. He, G. Li, X. Liu, C. Chen, B. Åkermark, L. Sun, Eur. J. Inorg. Chem. (2005) 2506.
[21] X. Zhao, I.P. Georgakaki, M.L. Miller, R. Mejia-Rodriguez, C.-Y. Chiang, M.Y. Darensbourg, Inorg. Chem. 41 (2002) 3917.
[22] K.G. Moloy, J.L. Petersen, J. Am. Chem. Soc. 117 (1995) 7696.
[23] M.L. Clarke, G.L. Holliday, A.M.Z. Slawin, J.D. Woollins, J. Chem. Soc. Dalton Trans. (2002) 1093.
[24] A.J. Bard, Electrochemical Methods: Fundamentals and Applications, Wiley, New York, 2001.
[25] I. Bhugun, D. Lexa, J.-M. Savéant, J. Am. Chem. Soc. 118 (1996) 3982.
[26] K. Nakamoto, Infrared and Raman Spectra of Inorganic and Coordination Compounds, Part B: Applications in Coordination, Organometallic, and Bioinorganic Chemistry, second ed., John Wiley & Sons, New York, 1997, pp. 126–148.
[27] S.J. Borg, T. Behrsing, S.P. Best, M. Razavet, X. Liu, C.J. Pickett, J. Am. Chem. Soc. 126 (2004) 16988.
[28] C.A. Boyke, T.B. Rauchfuss, S.R. Wilson, M.-M. Rohmer, M. Bénard, J. Am. Chem. Soc. 126 (2004) 15151.
[29] C.A. Boyke, J.I. van der Vlugt, T.B. Rauchfuss, S.R. Wilson, G. Zampella, L. De Gioia, J. Am. Chem. Soc. 127 (2005) 11010.
[30] J.I. van der Vlugt, T.B. Rauchfuss, C.M. Whaley, S.R. Wilson, J. Am. Chem. Soc. 127 (2005) 16012.
[31] M.H. Cheah, S.J. Borg, M.I. Bondin, S.P. Best, Inorg. Chem. 43 (2004) 5635.
[32] L.E. Bogan, D.A. Lesch, T.B. Rauchfuss, J. Organomet. Chem. 250 (1983) 429.
[33] Software packages SMRT and SAINT, Siemens Analytical X-Ray Instruments Inc., Madison, WI, 1996.
[34] SHELXTL, Version 5.1, Siemens Industrial Automation, Inc. 1997.
[35] S.G. Sun, in: J. Lipkowski, P.N. Ross (Eds.), Electrocatalysis, Frontiers of Electrochemistry, vol. 4, Wiley-VCH, New York, 1998 (Chapter 6).